Materials Research Express

PAPER • **OPEN ACCESS**

Performance evaluation of a new 30 μm thick GaAs x-ray detector grown by MBE

Materials Research Express

PAPER

Performance evaluation of a new 30 μm thick GaAs x-ray detector grown by MBE

G Lioliou[1], C L Poyser[2], J Whale[2], R P Campion[2], A J Kent[2] and A M Barnett[1]

[1] Space Research Group, School of Mathematical and Physical Sciences, University of Sussex, Brighton BN1 9QT, United Kingdom
[2] School of Physics and Astronomy, University of Nottingham, Nottingham NG7 2RD, United Kingdom

E-mail: G.Lioliou@sussex.ac.uk

Keywords: x-ray spectroscopy, photodiode, gallium arsenide, molecular beam epitaxy

OPEN ACCESS

RECEIVED
18 January 2021

REVISED
9 February 2021

ACCEPTED FOR PUBLICATION
17 February 2021

PUBLISHED
26 February 2021

Abstract

A circular mesa (400 μm diameter) GaAs p^+-i-n^+ photodiode with a 30 μm thick i layer was characterized for its performance as a detector in photon counting x-ray spectroscopy at 20 °C. The detector was fabricated from material grown by molecular beam epitaxy (MBE). An earlier MBE-grown detector fabricated using a different fabrication process and material from a different area of the same epiwafer was shown to suffer from: relatively high leakage current at high temperatures; a high effective carrier concentration that limited its depletion layer width; and material imperfections (butterfly defects) [Lioliou *et al* 2019 *Nucl. Instrum. Methods Phys. Res. A* **946** 162670]. However, the new detector has better performance (lower leakage current and effective carrier concentration within the i layer). Using the new detector and low noise readout electronics, an energy resolution of 750 eV ± 20 eV Full Width at Half Maximum (FWHM) at 5.9 keV was achieved at 20 °C, equal to that reported for high quality GaAs detectors made from high quality material grown by metalorganic vapour phase epitaxy [Lioliou *et al* 2017 *J. Appl. Phys.* **122** 244506]. The results highlight the substantially different performances of detectors made from the same epiwafer when the wafer qualities are not uniform and the effects of different fabrication processes.

1. Introduction

Applications both in space [1, 2] and on Earth [3] benefit from x-ray spectroscopy. Among the different semiconductor detectors employed in photon counting x-ray spectroscopy, GaAs (1.42 eV bandgap [4]) photodiodes are advantageous due to their radiation hardness [5, 6], high temperature tolerance [7], and good stopping power for x-ray photons of up to moderate energy [8]. Considerable efforts have been made to grow thick GaAs structures to increase the quantum detection efficiency of such detectors while maintaining material quality, and hence, performance [7, 9].

Chemical vapor phase deposition (CVPD) techniques, including metalorganic vapour phase epitaxy (MOVPE), are common growth techniques for thick GaAs photodiode structures [7, 10]. However, investigation of molecular beam epitaxy (MBE) for growing high-quality thick GaAs structures, such as x-ray detectors, is interesting due to the relative simplicity of its epitaxial growth concept, which makes MBE a powerful technique with unparalleled control and reproducibility. It should be noted that each of the two epitaxial techniques has its advantages and limitations, making them the preferred choice for different device applications. A thick GaAs p^+-i-n^+ mesa photodiode (30 μm thick i layer) fabricated from an epiwafer grown by MBE was recently reported; a modest energy resolution was achieved (860 eV Full Width at Half Maximum, FWHM, at 5.9 keV at 20 °C, improving to 730 eV FWHM at 5.9 keV at −20 °C) when coupled to a low noise charge sensitive preamplifier and regular onwards readout electronics [11]. That packaged detector had relatively high leakage current (e.g. 23.2 pA at 20 °C) and capacitance (e.g. 2.2 pF at 20 °C) which contributed to the broadening of the FWHM. The detector also suffered from: the presence of butterfly defects (material imperfections having a characteristic butterfly shape) which arose during the epitaxial growth possibly from the creation of unwanted non-integer step heights on the surface and were non-uniformly distributed [11]; a limited

depletion of the intrinsic layer due to high carrier concentrations in what was intended to be the unintentionally doped i layer; and possibly surface leakage current over the mesa side walls which contributed to the measured leakage current [11].

Here, results are reported which characterize a new GaAs p^+-i-n^+ x-ray photodiode. Electrical characterization and ^{55}Fe x-ray spectroscopy results and analysis are presented for the new detector along with those obtained with the old detector [11] to enable easy comparisons.

2. Methods

2.1. Detector structure

The new detector was fabricated from the same epiwafer as was used for the earlier detector and it was of identical geometry to its predecessor [11]. However, the material used was selected from a different area of the wafer (also having butterfly defects with varied density across the surface) and a refined fabrication process was employed. As reported in [11], the p^+-i-n^+ epi-structure was grown on a commercial n^+ GaAs substrate. The growth rate was 1 μm h^{-1} and the epiwafer growth temperature was 610 °C. The p^+ layer (0.5 μm thick) was doped with C and the n^+ layer (1 μm thick) was doped with Si, both at a doping density of 2×10^{18} cm^{-3}. A 10 nm thick p^+ contact layer (1×10^{19} cm^{-3} doping density) was grown atop the p^+ layer. The new circular mesa (400 μm diameter) photodiode was wet etched from the wafer: H_3PO_4:H_2O_2:H_2O (1:1:1) was used for 20 min to fully etch the mesa down to the substrate (an etch depth ≈40 μm was achieved). A finishing etch in H_2SO_4:H_2O_2:H_2O (1:8:80) for 2 min was then performed. The previously reported GaAs x-ray detector was only partially etched and did not have the finishing etch [11]. A quasi-annular Ohmic contact (15 nm Au; 30 nm Zn; 150 nm Au) was formed, by evaporation, on the top of the detector (covering 11% of its face). A rear 100% coverage Ohmic contact (10 nm Ge; 45 nm Au; 15 nm Ni; 150 nm Au) was evaporated onto the back of the substrate. The photodiode was packaged in a TO-5 can and wire bonded in the same way as the previous detector [11].

2.2. Experimental procedures

The electrical characterization included leakage current and capacitance measurements. Measurements of the leakage current and capacitance of an x-ray detector are fundamental parts of its characterization since they both contribute to the noise of the x-ray spectrometer employing the detector and, in part, determine the energy resolution achieved. The new detector was installed inside a TAS Micro LT225 climatic cabinet to maintain its temperature at 20 °C. The leakage current and the capacitance of the new detector was measured as a function of reverse bias up to −100 V, which was applied in both cases using a Keithley 6487 Picoammeter/Voltage Source. The leakage current was measured using the Keithley 6487 Picoammeter/Voltage Source and the capacitance was measured using an HP Multi Frequency LCR meter, with 50 mV rms magnitude and 1 MHz frequency test signal.

The x-ray spectroscopic performance of the new GaAs detector was then investigated. The detector was coupled to a custom-made charge sensitive preamplifier of the same design as was used with the old detector [11], which was of a feedback-resistorless design similar to [12]. The preamplifier was then connected to an ORTEC 572 A shaping amplifier and an ORTEC EASY MCA 8k multi-channel analyser (MCA). An ^{55}Fe radioisotope x-ray source (101 MBq activity; giving Mn Kα (5.9 keV) and Mn Kβ (6.49 keV) characteristic emission lines [13]) was placed above the detector. ^{55}Fe x-ray spectra were accumulated at all available shaping times, τ, (0.5 μs, 1 μs, 2 μs, 3 μs, 6 μs, and 10 μs), at detector reverse biases of −10 V and −50 V.

3. Results and discussions

3.1. Electrical characterization

The results of the leakage current and capacitance measurements are presented in figure 1. The new detector had a leakage current of 38.3 pA ± 0.7 pA at −100 V reverse bias, which was lower than that of the old detector (111.2 pA ± 0.8 pA) at the same applied reverse bias. This was partly attributed to the use of the H_2SO_4:H_2O_2:H_2O finishing etch, which is thought to have supressed the surface leakage current (arising from the mesa sidewalls); similar leakage current reductions attributable to the use of H_2SO_4:H_2O_2:H_2O finishing etches have been reported previously for other GaAs [14] and InAs [15] mesa photodiodes. The capacitance of the new detector reduced from 6.16 pF ± 0.01 pF at 0 V to 0.584 pF ± 0.006 pF at −100 V; this suggested that the i layer was not fully depleted at the maximum investigated applied reverse bias. The measured capacitance of the new detector at −100 V (0.6 pF ± 0.1 pF) was lower than that of the old detector (1.0 pF ± 0.1 pF) at the same applied reverse bias.

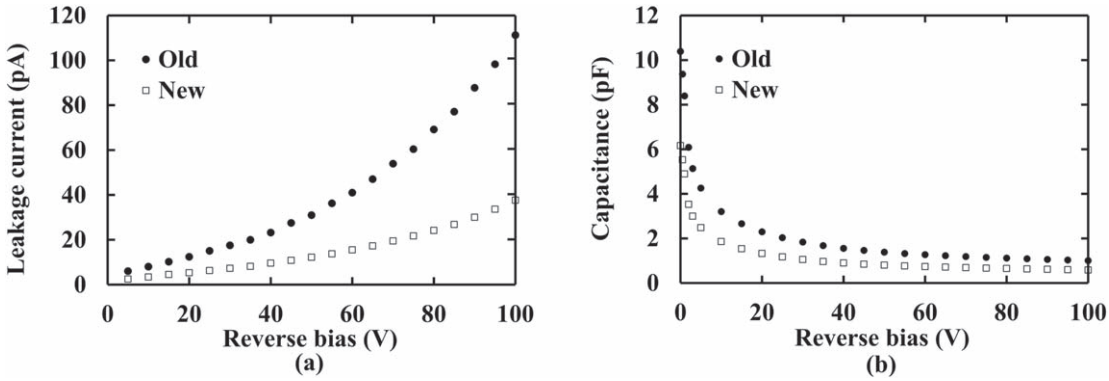

Figure 1. (a) Leakage current and (b) capacitance of the new (open squares) and old (filled circles) [11] detectors at 20 °C as functions of applied reverse bias.

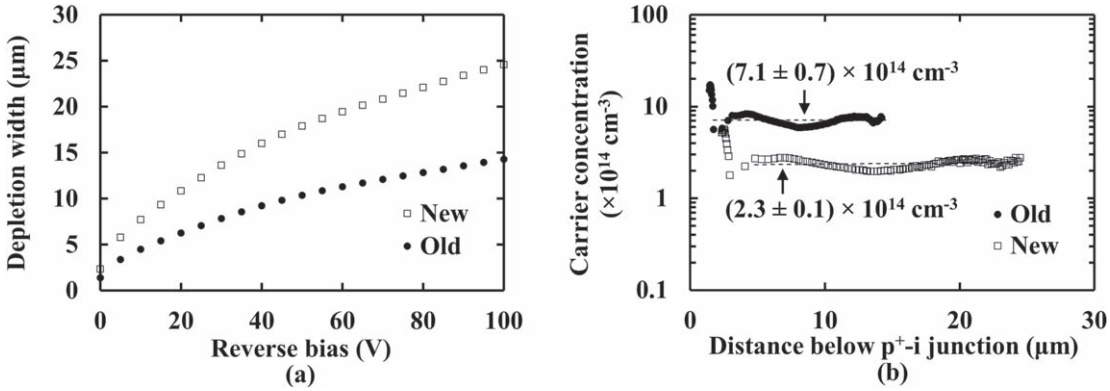

Figure 2. (a) Depletion widths as functions of applied reverse bias and (b) effective carrier concentration as a functions of distance below the p-i junction for the new (open squares) and old (filled circles) detectors. The mean effective carrier concentrations within each i layer are also shown (dashed lines).

The depletion width and the effective carrier concentration within the i layer were determined from the capacitance measurements (figure 1(b)) and are presented in figure 2. The depletion width of the new detector increased from 7.7 μm ± 0.5 μm at −10 V to 18 μm ± 2 μm at −50 V, and to 25 μm ± 4 μm at −100 V applied reverse bias. The apparent slight variation of the effective carrier concentration between 5 μm and 25 μm (corresponding to the maximum investigated, −100 V, applied reverse bias) below the p^+-i junction (figure 2(b)), was not real; the effective carrier concentration was constant (within uncertainties) from 5 μm to 25 μm below the p^+-i junction, with a mean value, as determined by the *y*-axis intercept point of the line of best fit (calculated using linear least squares fitting), of 2.3×10^{14} cm^{-3} ± 0.1×10^{14} cm^{-3}. This is similar to that reported for GaAs p^+-i-n^+ photodiodes fabricated from high quality material grown by MOVPE [7] and CVPD [16] (≈1.5×10^{14} cm^{-3}). In contrast, the old GaAs detector had an apparent mean effective carrier concentration within the i layer of 7.1×10^{14} cm^{-3} ± 0.7×10^{14} cm^{-3}, which limited its depletion layer width to 14 μm ± 1 μm at −100 V reverse bias [11]. As such, it can be interpreted that there was significant variation in effective carrier concentration across the wafer.

3.2. ^{55}Fe x-ray spectroscopy and noise analysis

An example ^{55}Fe x-ray spectrum accumulated with the x-ray spectrometer using the new detector can be seen in figure 3. The energy resolution of the x-ray spectrometer was not sufficient to resolve the individual Mn Kα and Mn Kβ peaks, thus the combination of the Mn Kα and Mn Kβ peaks was detected. Gaussian peaks, centred at 5.9 keV and 6.49 keV, were fitted to the combined peak, given due consideration to the x-ray emission probabilities of ^{55}Fe [13], the engineering characteristics of this specific ^{55}Fe radioisotope x-ray source's encapsulation, and the relative quantum efficiency of the detector at those energies. The position (centroid channel number) of the Gaussian corresponding to the 5.9 keV photopeak was used along with the zero energy noise peak to calibrate the MCA scale of each spectrum in energy terms. The energy resolution (FWHM at 5.9 keV) was then recorded.

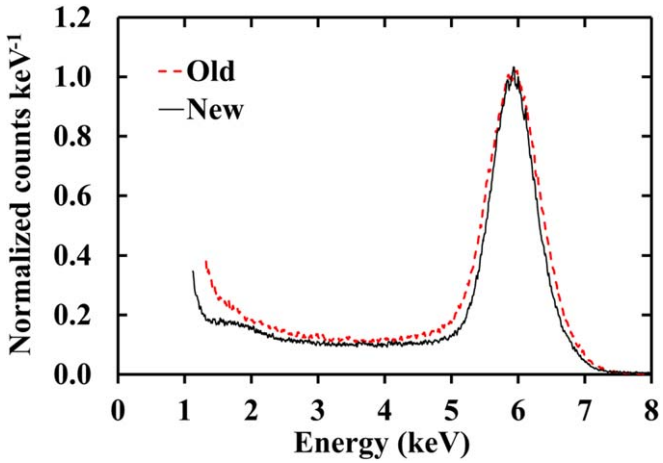

Figure 3. ^{55}Fe x-ray spectra accumulated with the new detector (black solid line) (−50 V reverse bias; 2 μs shaping time; 750 eV ± 20 eV FWHM at 5.9 keV) and the old detector (red dashed line) (−40 V reverse bias; 0.5 μs shaping time; 860 eV FWHM at 5.9 keV) [11]. The spectra were normalised to the height of the fitted Gaussian corresponding to the Mn Kα peak (not shown).

The ^{55}Fe x-ray spectrum accumulated with the spectrometer using the new detector, operated at the conditions (−50 V reverse bias; 2 μs shaping time) which gave the best (lowest) FWHM, is shown in figure 3. An energy resolution of 750 eV ± 20 eV FWHM at 5.9 keV was recorded. The MCA's low energy cut off was set at an energy >0 keV (e.g. at 1.1 keV for the spectrum shown in figure 3) to limit the number of counts in the zero energy noise peak. The corresponding spectrum accumulated with the old detector is also presented; the different count rates and MCA channel widths of the two spectra were taken into account by normalizing the peak heights and presenting the spectra in terms of counts keV^{-1} (cf counts channel^{-1}). The low energy tailing at the left hand side of the ^{55}Fe x-ray photopeaks seen in figure 3 was attributed to partial charge collection of charge created in the non-active regions of the devices. The additional peak at the right hand side of the zero energy noise peak (counts at energies, E, 1 keV $\lessapprox E \lessapprox$ 2 keV) are attributed to detector self-fluorescence: Ga Lα (1.098 keV) and Lβ (1.125 keV); As Lα (1.282 keV) and Lβ (1.317 keV).

The energy resolution achieved (750 eV ± 20 eV FWHM at 5.9 keV) was better than that achieved with the old detector at 20 °C (860 eV FWHM at 5.9 keV [11]). Additionally, the energy resolution of the new detector at 20 °C was similar to that obtained with MOVPE-grown GaAs detectors at 20 °C when coupled to similar electronics (730 eV FWHM at 5.9 keV [7]), and also similar to that obtained with the old MBE-grown detector when it was cooled to −20 °C (730 eV FWHM at 5.9 keV [11]). These results are discussed in the next paragraphs.

The FWHM at 5.9 keV was defined by the quadratic sum of three independent noise contributions, the Fano noise, any incomplete charge collection noise, and the electronic noise [17]. The Fano noise, the incomplete charge collection noise, and part of the electronic noise ($1/f$ and dielectric) are all shaping time invariant. However, part of the electronic noise varies with shaping time: the white series (*WS*) noise is inversely proportional to shaping time; the white parallel (*WP*) noise is proportional to shaping time. Thus, a multidimensional nonlinear minimization to the measured FWHM at 5.9 keV as a function of shaping time allowed the identification of the components that were: shaping time invariant (quadratic sum of Fano, incomplete charge collection, $1/f$, and dielectric noise); inversely proportional to shaping time (*WS*); and proportional to shaping time (*WP*). The FWHM at 5.9 keV achieved with the new detector, and the Equivalent Noise Charge (ENC) as a function of shaping time at the two applied reverse biases investigated, along with the corresponding multidimensional least squares fittings, can be seen in figure 4.

The total leakage current at the input of the preamplifier contributed to the white parallel noise and the total capacitance at the input of the preamplifier contributed to the white series noise [17]. Even though the white parallel noise increased as the applied reverse bias increased in magnitude, from −10 V to −50 V, a better energy resolution was achieved at −50 V cf that at −10 V. This was attributed to the reduction of both the white series noise and the τ invariant component of the noise at the highest applied bias (figure 4). The dominant source of noise within the investigated shaping time range was the τ invariant component (quadratic sum of Fano noise, any incomplete charge collection noise, $1/f$ noise, and dielectric noise); it reduced from 73 e^- rms at −10 V to 69 e^- rms at −50 V. The Fano noise (assuming an average electron hole pair creation energy of 4.19 eV [4] and a Fano factor of 0.12 [16]) and the $1/f$ noise [17] were calculated and subtracted in quadrature from the τ invariant noise component to give the combined contribution (quadratic sum) of any incomplete charge collection noise and the dielectric noise. The quadratic sum of any incomplete charge collection noise and the dielectric noise reduced by 23 e^- rms, from 71 e^- rms at −10 V to 67 e^- rms at −50 V. The dielectric noise contribution of the GaAs detector was proportional to

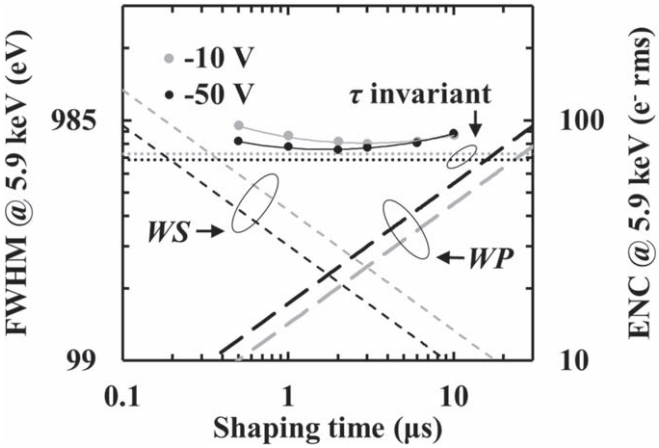

Figure 4. Measured FWHM and ENC at 5.9 keV (filled circles) as a function of shaping time at −10 V (grey symbols) and −50 V (black symbols) reverse bias. Shown are the noise contributions determined from a multidimensional least squares fitting (solid lines) of the experimental data (filled circles): white series, *WS*, (short dashed lines); white parallel, *WP*, (long dashed lines); τ invariant components i.e. quadratic sum of Fano noise, any incomplete charge collection noise, $1/f$ noise, and dielectric noise (dotted lines).

its capacitance [17] and thus it was expected to reduce at −50 V cf that at −10 V applied reverse bias; a reduction of 9 e^- rms, from 11 e^- rms at −10 V to 7 e^- rms at −50 V, was calculated considering the change in detector capacitance (figure 1(b)) and assuming a dielectric dissipation factor of 2×10^{-4} for GaAs [18, 19]. The rest of the reduction of the quadratic sum of the incomplete charge collection noise and the dielectric noise at −50 V cf that at −10 V, equal to 22 e^- rms, was attributed to the reduction of the incomplete charge collection noise at increased applied electric field strength, due to improved charge transport. Further increases in applied reverse bias magnitude may have resulted in additional reductions in incomplete charge collection noise but this could not be investigated due to restrictions in laboratory access during the COVID-19 pandemic.

The difference between the energy resolutions (FWHM at 5.9 keV) achieved with the new and old GaAs detectors, corresponding to an ENC difference of 43 e^- rms, was partly attributed to reductions in the contributions of: white parallel noise (lower leakage current, figure 1(a)); white series noise (lower capacitance, figure 1(b)); and dielectric noise (lower capacitance, figure 1(b)) for the new cf old detector. The quadratic sum of these noise components was calculated for each detector; it was 19 e^- rms for the new detector (−50 V applied reverse bias; 2 μs shaping time) and 24 e^- rms for the old detector (−40 V applied reverse bias; 0.5 μs shaping time), suggesting a difference of 14 e^- rms. The remainder in the difference between the ENC of the two detectors (41 e^- rms) appears to suggest better charge collection efficiency (i.e. lower incomplete charge collection noise) in the new detector, since there were no other significant differences which could have accounted for the improvement.

Although the incomplete charge collection noise contribution when the new detector was operated at an applied reverse bias of −50 V cannot be readily calculated, a significant difference in the characteristics of the old and new detectors was observed. Measurements with the old detector operated at applied reverse biases from −10 V to −100 V, suggested that any improvement in (reduction of) incomplete charge collection noise was negligible over that bias range [11]. This was in contrast with the new detector where a substantial improvement (22 e^- rms) was seen as the reverse bias applied to the detector was increased from −10 V to −50 V. As such, if the improvement in the new cf old detector as described above was due to less incomplete charge collection noise in the new detector, it appears that the charge trapping in the old detector was so significant as to be unaffected by increased electric field strength within the range investigated [11].

The number of counts within the fitted Mn Kα (5.9 keV) Gaussian peak at −50 V was a factor of 1.8 ± 0.1 greater than the number of counts in the same peak at −10 V. Such an increase was larger than would have been predicted considering the Beer–Lambert law and the measured deletion layer widths at those reverse biases (figure 2(a)): based on the change in depletion layer width, the number of counts in the Mn Kα peak at −50 V would have been predicted to be a factor of 1.5 ± 0.1 greater than that at −10 V. The apparently supernumerary increase in efficiency may indicate that the charge collection in the detector's depleted region at −10 V applied reverse bias was substantially incomplete. An alternative explanation, i.e. that there was, at −50 V, a disproportionate increase in the substantially complete collection of charge from the region below the depleted region by virtue of that charge diffusing to the depleted region is considered unlikely to be true. It would have required the significantly complete collection of charge from a 38 μm thick GaAs layer; considering the layer structure of the GaAs photodiode, this would require charge (holes) created within the n^+ layer (1 μm thick) and the top 6.5 μm of the n^+ substrate to diffuse to the depleted region. However, the hole diffusion length in a highly

doped (2×10^{18} cm^{-3}) n^+ type GaAs is ≈1 μm [20]. As such, the explanation that charge collection was significantly incomplete at −10 V applied reverse bias is considered to be the likely explanation.

4. Conclusion

Summarizing, a new GaAs p^+-i-n^+ mesa photodiode (30 μm thick i layer) fabricated from material grown by MBE was used as a spectroscopic x-ray detector at a temperature of 20 °C. The detector had substantially different performance compared to a previously reported detector made from a different area of the same epiwafer using a different fabrication procedure [11]. An energy resolution of 750 eV ± 20 eV FWHM at 5.9 keV was achieved; this was substantially better than with the old detector (860 eV FWHM at 5.9 keV) and similar to that achieved with high quality MOVPE-grown GaAs detectors connected to comparable readout electronics (730 eV FWHM at 5.9 keV [7]). An improvement in the charge collection efficiency was observed as the applied reverse bias to the detector was increased from −10 V to −50 V. Nevertheless, uncertainty still remains about the exact nature and extent of incomplete charge collection noise in the MBE-grown detectors and work is required to improve the epitaxial material quality across the wafer.

Acknowledgments

This work was supported by the Science and Technology Facilities Council, United Kingdom, through grants ST/P001815/1 and ST/R001804/1 (University of Sussex, A M B, PI). A M B acknowledges funding from The Leverhulme Trust, United Kingdom, in the form of a 2016 Philip Leverhulme Prize.

Data availability statement

All data that support the findings of this study are included within the article.

ORCID iDs

G Lioliou https://orcid.org/0000-0002-6989-7106
A J Kent https://orcid.org/0000-0002-2391-6869

References

[1] Fraser G W *et al* 2010 *Planet. Space Sci.* **58** 79–95
[2] Grande M *et al* 2009 *Planet. Space Sci.* **57** 717–24
[3] Procz S, Avila C, Fey J, Roque G, Schuetz M and Hamann E 2019 *Radiat. Meas.* **127** 106104
[4] Bertuccio G and Maiocchi D 2002 *J. Appl. Phys.* **92** 1248–55
[5] Ly Anh T, Perd'ochová A, Nečas V and Pavlicová V 2006 *Nucl. Phys. B Proc. Suppl.* **150** 402–6
[6] Rossi L, Fischer P, Rohe T and Wermes N 2006 *Pixel Detectors: From Fundamentals to Applications* (Berlin: Springer)
[7] Lioliou G, Whitaker M D C and Barnett A M 2017 *J. Appl. Phys.* **122** 244506
[8] Seltzer S M 1993 *Radiat. Res.* **136** 147–70
[9] Owens A, Peacock A J and Bavdaz M 2003 *Proc SPIE* **4851** 1059–70
[10] Owens A, Bavdaz M, Peacock A, Poelaert A, Andersson H, Nenonen S, Tröger L and Bertuccio G 2001 *Nucl. Instrum. Methods Phys. Res. A* **466** 168–73
[11] Lioliou G, Poyser C L, Butera S, Campion R P, Kent A J and Barnett A M 2019 *Nucl. Instrum. Methods Phys. Res. A* **946** 162670
[12] Bertuccio G, Rehak P and Xi D 1993 *Nucl. Instrum. Methods Phys. Res. A* **326** 71–6
[13] Schötzig U 2000 *Appl. Radiat. Isot.* **53** 469–72
[14] Ng J S, Meng X, Lees J E, Barnett A M and Tan C H 2014 *J. Instrum.* **9** T08005
[15] Marshall A R J, Tan C H, David J P R, Ng J S and Hopkinson M 2007 *Proc. SPIE* **6740** 67400H
[16] Bertuccio G, Casiraghi R, Maiocchi D, Owens A, Bavdaz M, Peacock A, Andersson H and Nenonen S 2003 *IEEE Trans. Nucl. Sci.* **50** 723–8
[17] Lioliou G and Barnett A M 2015 *Nucl. Instrum. Methods Phys. Res. A* **801** 63–72
[18] Courtney W E 1997 *IEEE Trans. Microw. Theory Tech.* **25** 697–701
[19] Krupka J, Mouneyrac D, Hartnett J G and Tobar M E 2008 *IEEE Trans. Microw. Theory Tech.* **56** 1201–6
[20] Hwang C J 1971 *J. Appl. Phys.* **42** 4408–13